The impact of surface roughness geometry on aero-engine intakes at incidence

C. Coles* and H. Babinsky †

Department of Engineering, University of Cambridge, Cambridge, CB2 1PZ, UK

E. Platt ‡ and C.Sheaf ‡

Installation Aerodynamics, Rolls Royce Plc., Derby, DE24 8BJ, UK

Shock Wave-Boundary-Layer Interactions, or SBLI's, are known to form on engine inlets within a complex transonic flow-field during typical take-off and climb configurations. On the engine inlet, there are a number of potential sources of surface roughness, such as novel de-icing and acoustic systems, or surface contamination. The impact on the flow-field structure, as a result of this roughness, may lead to detrimental side effects, such as losses in engine efficiency or intake flow stability. Previous research into two-dimensional roughness shapes demonstrated flow-field changes, for example a thicker downstream-boundary layer compared to a smooth surface. This paper compares the impact of a two-dimensional ridge roughness to a three-dimensional cubed roughness on the inlet flow-field. The effect of these rough surfaces is examined with schlieren photography and Laser Doppler Velocimetry (LDV) techniques. At an on-design condition, a rough surface promotes a smaller supersonic region, and a thicker boundary-layer downstream of the interaction compared to a smooth surface. At off-design upper surface mass flow rate conditions, modelling a higher mass flow engine demand, the supersonic region grows, leading to a shock location further downstream. Under these conditions, roughness also promotes a thicker downstream boundary-layer. However, comparing the two-dimensional with three-dimensional roughness at an approximate fan-face location, shows that three-dimensional roughness is more benign for all off-design cases. This suggests that the topology of the roughness is influencing the condition of the boundary-layer at this location.

Nomenclature

d_1	Streamwise width of 2D and 3D roughness elements
d_2	Spanwise width of 3D roughness element
k	Roughness element height
k^+	Non-dimensional roughness element height
$\dot{m}_{upper}$	Mass flow rate in upper channel
$\dot{m}_{entry}$	Mass flow rate at entry to working section
M_{entry}	Mach number at entry to working section
P_0	Stagnation Pressure
Re	Reynolds number
S	Streamwise coordinate
t	Maximum Lip thickness
T_0	Stagnation Temperature
U	Velocity
U_e	Free Stream Velocity
X	Horizontal coordinate

*PhD Student, Department of Engineering, University of Cambridge.

†Professor of Aerodynamics, Department of Engineering, University of Cambridge, AIAA Associate Fellow.

‡Installation Aerodynamics, Rolls Royce Plc, Derby.

y	Distance from surface
α	Angle of incidence of model
δ	Boundary-layer thickness
δ_i^*	Incompressible displacement thickness
θ_i	Incompressible momentum thickness
H_i	Incompressible shape factor, δ_i^*/θ_i
δ_s	Boundary-layer thickness, smooth surface
$\delta_{i,s}^*$	Incompressible displacement thickness, smooth surface
$\theta_{i,s}$	Incompressible momentum thickness, smooth surface
λ	Distance between roughness elements
u_τ	Friction Velocity
ν	Kinematic Viscosity
ρ	Density
CAD	Computer Aided Design
LDV	Laser Doppler Velocimetry
SBLI	Shock Wave-Boundary-Layer Interaction

I. Introduction

At high angles of incidence, for example during conditions typical of aircraft take-off or climb configurations, the flow around the nacelle lip accelerates to a supersonic value. This creates a supersonic region, which is then terminated by a shock wave. At the base of this shock wave is a shock wave-boundary-layer interaction, or SBLI. A schematic of this flow-structure is shown in Fig. 1.

Previous studies, such as those by Coschignano,[1] have investigated purely smooth nacelle surfaces at different operating conditions. However, surface roughness could be presented to the flow in a variety of ways. For example, surface contamination from bugs adhering to the surface, ice formation, or due to features such as novel acoustic or de-icing systems. While the aerodynamic effects of surface roughness have been studied for many years, little is known about their influence on transonic SBLI's and, in particular, their effect around the inlet lip. One concern is that the roughness may alter the flow-field structure or cause premature flow separation. This in turn, could cause detrimental effects, such as losses in engine efficiency and intake aerodynamic flow instability.

Initial studies[2] of roughness effects have identified changes to the flow structure, for example increasing the boundary-layer thickness downstream of the SBLI on the inlet lip. However, these studies have only considered an idealistic two-dimensional roughness shapes, whereas a more realistic topology is likely to be three-dimensional. Therefore, this paper aims to compare a large-scale two-dimensional (2D) "ridge" roughness with a three-dimensional (3D) "cubed" roughness and their impact on the inlet flow-field.

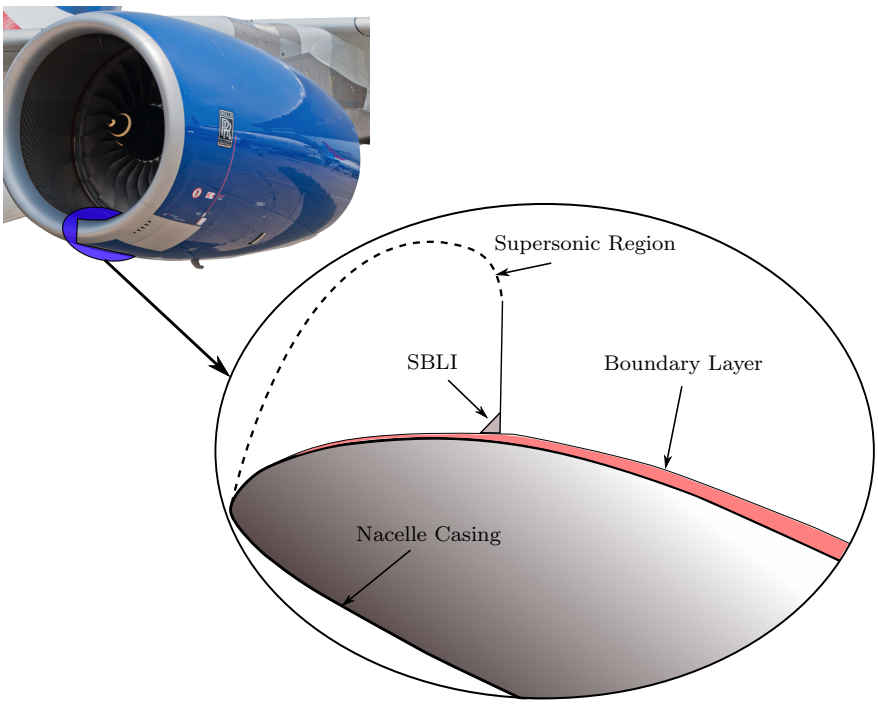

Figure 1. Schematic of flow-field. Insert of Trent 700[3]

II. Experimental Set-up and Methodology

II.A. Experimental Rig

Experiments are undertaken in the blow-down supersonic wind tunnel in the Cambridge University Engineering Department. The tunnel is supplied with air from two 50kW compressors. The pressurised air passes through a settling chamber, containing turbulence grids and flow straighteners, into an 18:1 contraction. The flow then enters the custom-made working section, designed by Makuni[4] to investigate transonic flow over the inside surface of a nacelle lip at incidence conditions. The upper and lower walls of the working section create a streamtube. The streamtube was extracted from a 3D computation of the transonic flow field into an engine inlet at typical take off conditions.

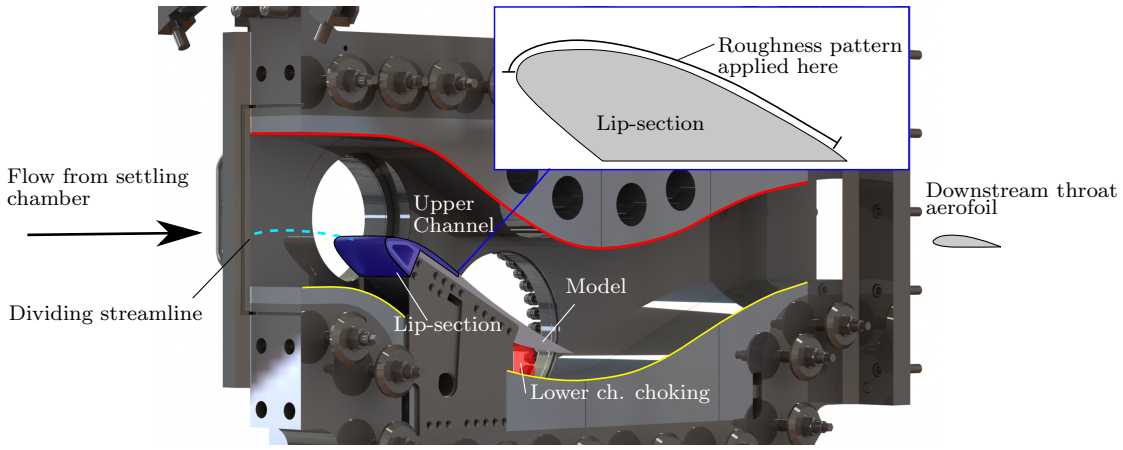

Figure 2. Setup of working section. Adapted from Coschignano et al.[1]

Inside the working section sits the intake model, identified in Fig. 2. The engine leading edge geometry is replicated by an aerofoil-shaped model. The nose geometry of this model is similar to current nacelle

designs, and is sized at roughly 1/7th of the full-scale. The upper wall of the working section is designed to be far enough away from the intake model to prevent choking in the upper channel.[1]

The overall mass flow rate into the working section, $\dot{m}_{entry}$, and the incoming Mach number, M_{entry}, are set by the downstream throat aerofoil and the stagnation pressure in the settling chamber. These are both identified in Fig. 2. The lower channel mass flow rate is set by adjusting the lower channel choking area. This then implicitly sets the upper channel mass flow rate $\dot{m}_{upper}$. Changing the upper channel mass flow rate allows operating conditions akin to changing the engine mass flow demand to be tested.

For typical inflow conditions, the Reynolds number based on maximum lip thickness is approximately 10^6. This matches full-scale conditions for a smaller engine at about 3000m in altitude, within the take off regime. Previous measurements for this set-up have confirmed the free stream turbulence levels to be less than 1%.[1]

The on-design operating condition is listed in table 1. This condition closely mimics a target flow provided by Rolls-Royce from both experimental and computational results based on a real intake at incidence. Subsequent changes to the upper channel mass flow, $\dot{m}_{upper}$, alters the position of the stagnation streamline around the intake model and allows off-design mass flow rate conditions, representative of a high mass flow demand, to be replicated. Four upper channel mass flow rates ($\dot{m}_{upper}$), have been tested, called Low, Medium, Moderate and High. Low is the on-design $\dot{m}_{upper}$ condition, and Medium, Moderate and High are off-design $\dot{m}_{upper}$ conditions. The respective upper channel mass flow rates for each of these conditions are listed in table 2.

Table 1. On-design conditions

M_{entry}	$\dot{m}_{upper}$	α(deg.)	P_0(kPa)	T_0(K)	Re
0.435	$0.736\dot{m}_{entry}$	23	211.6	290±4	10^6

Table 2. Upper channel mass flow rate levels

Level	$\dot{m}_{upper}$
Low (on-design)	0.736 $\dot{m}_{entry}$
Middle	0.749 $\dot{m}_{entry}$
Moderate	0.762 $\dot{m}_{entry}$
High	0.776 $\dot{m}_{entry}$

The intake model is made of a number of constituent parts. A key geometry, called "the lip-section", is highlighted in blue in Fig. 2. A CAD model of the smooth lip-section has artificial roughness elements added to it, to create a new rough shape. The roughness elements cover the width of the lip-section, and extend streamwise from the nose to a similar position to the fan face on a real engine. The roughened lip-section is then manufactured by 3D-printing.

Two types of surface roughness are used on the model, one is a two-dimensional ridge structure, investigated previously[2] with an element roughness height, k, of $100\mu m$, and a ratio of element separation to height of $\lambda/k = 10$. The width of each element, d_1 is 0.25mm. The second roughness surface is a three-dimensional roughness, with cubes over the surface. These have an element height of k=$100\mu m$, size d_1= 0.25mm and d_2=0.25 mm, and a $\lambda/k = 10$. A schematic of the 2D and 3D roughness is shown in Fig. 3.

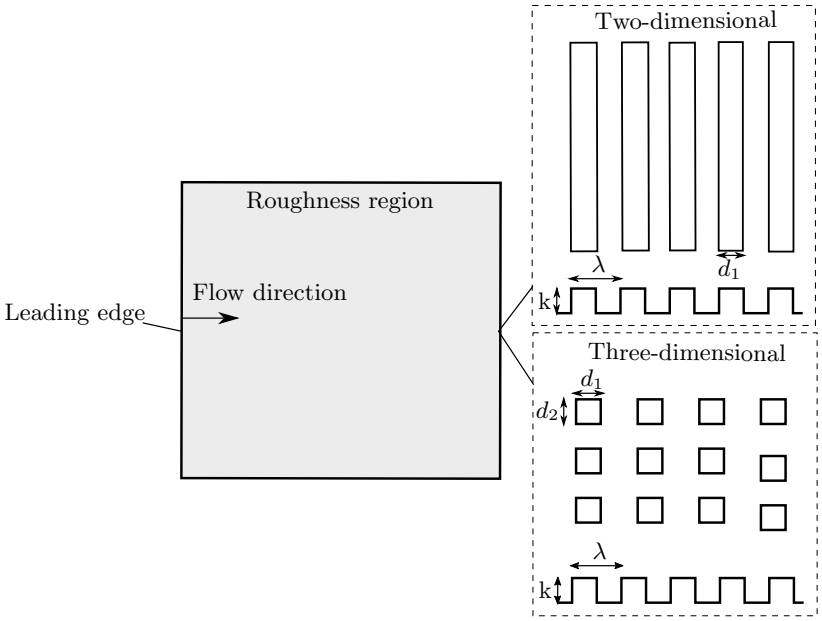

Figure 3. Plan view schematic of rough surfaces.

The rough lip-sections are characterised by the non-dimensional roughness height k^+, the definition of which can be found in equation 1.

$$k^+ = u_\tau k/\nu \tag{1}$$

The values of the friction velocity, u_τ, and the kinematic viscosity, ν, are extracted from a computation[5] of the same rig and operating condition. An example shear stress distribution on the smooth aerofoil model is shown in Fig. 4. Downstream of the shock wave-boundary-layer interaction (SBLI), the values of shear stress do not fluctuate greatly. Therefore, an average of the shear stress, u_τ and ρ was taken between 23% to 54% of the aerofoil length, downstream of the interaction. For both the 2D and 3D rough surfaces, this produces a k^+ of 92.9.

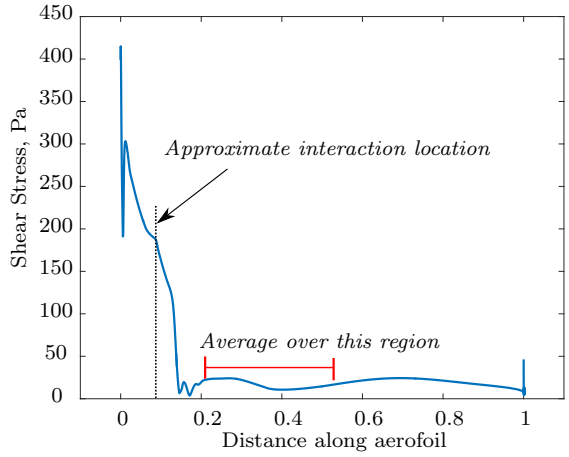

Figure 4. Plot of shear stress distribution over intake model[5]

II.B. Experimental Methods

A number of qualitative and quantitative methods are used to investigate the flow. Schlieren photography visualises the supersonic flow-field, and highlights supersonic features. The schlieren used is a 'z-type' system, with a horizontal knife edge placed in-front of the recording camera. This camera captures 4000 frames in one second. An example schlieren image is shown in Fig. 5.

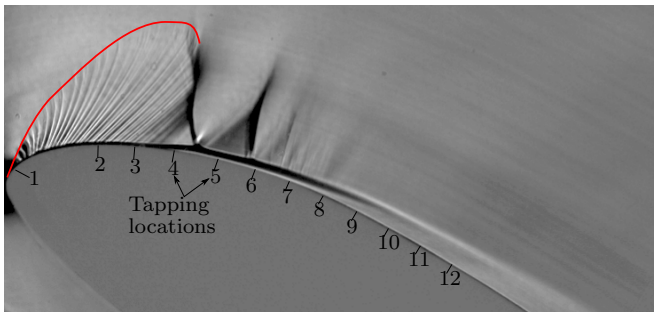

Figure 5. Example of schlieren technique for flow visualisation, with pressure tapping locations.

Pressure measurements are taken from a number of centreline surface pressure tappings, as highlighted in Fig. 5. These twelve tappings extend from the approximate stagnation position at the nose of the lip-section, equally spaced at 1cm intervals over the surface. The tappings themselves are small holes, 0.5mm in diameter, connected to a pressure transducer via tubing. The measured pressure values at each tapping are used to create a pressure distribution over the lip-section surface. The pressure distributions can then be compared at each operating condition, and between different runs, to ensure repeatability.

Velocity measurements are recorded by Laser Doppler Velocimetry (LDV). This is a two-component system, with lasers whose wavelengths are 542nm and 532nm respectively. These are focused inside the working section at a desired location. This produces an elliptical working volume of $130\mu m$ in diameter. During the run, the working section is seeded with kerosene particles typically of diameter no greater than $0.5\mu m$ in diameter. The emitting head of the laser and the receiving optical equipment is mounted on a traverse.

LDV results are recorded at the location S2, a location equivalent to the fan-face location on the real engine, from which the boundary layer profile is extracted, and horizontally across the shock. These locations are indicated in Fig. 6.

An analytical expression for a turbulent boundary-layer is applied to the measured boundary-layer traverses, combining a Sun and Childs[6] profile in the middle and wake regions of the boundary-layer, with a Musker[7] curve near the wall. This allows the extraction of the boundary-layer properties from this fitted curve, and avoids the introduction of significant errors due to poor near wall resolution.[8] The parameters extracted are the incompressible displacement thickness (δ_i^*), the incompressible momentum thickness (θ_i) and incompressible shape factor (H_i), as well as an estimation of the boundary-layer thickness (δ). A source of error for the LDV system is finding the location of the surface for each boundary-layer traverse. By bringing the working volume closer to the surface, reflections from the surface can be seen in the receiving optics. When these reflections reach the working volume, the surface has been found. This is found to be accurate to within $\pm$0.1mm.

The stagnation temperature is recorded by using T-type thermocouples, placed in the settling chamber. Any variation in stagnation temperature during a run is accounted for when converting the absolute velocity measurements from LDV to Mach number. This reduces the error in Mach number, which would peak at 1.7%,[1] if not considered.

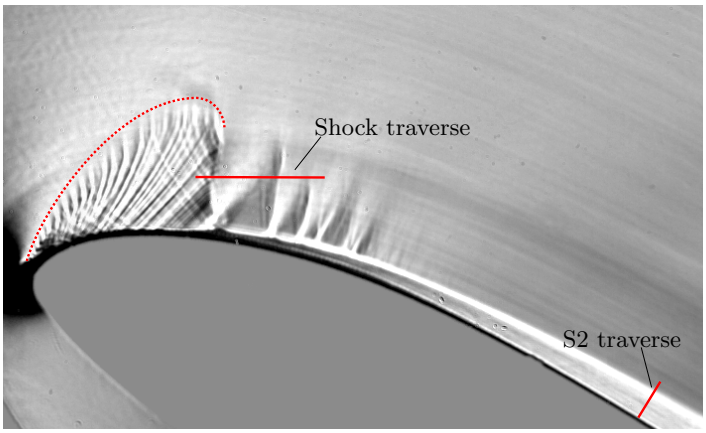

Figure 6. Location of S2 traverse and shock traverse

III. Results

III.A. On-design Conditions

At the on-design condition, the 2D rough lip-section and 3D rough lip-section exhibit a similar flow-field as the smooth lip-section, which is shown in Fig. 7 as reference.

The flow-field for the 2D rough and 3D rough lip-sections are shown in Fig. 8 and Fig. 9 respectively. It can be seen that the supersonic region for the 2D and 3D rough lip-sections is smaller and, the shock location is more upstream than in the smooth baseline case. The two rough lip-sections have a similarly sized supersonic region, resulting in a similar shock location.

At the base of the shock, for both smooth and rough surfaces, the presence of a λ-foot is indicative of separation, and this separation appears to be larger with the presence of roughness. Downstream of this interaction, the schlieren images suggest a thicker boundary-layer for both the rough lip-sections, compared to the smooth case. Also downstream of the interaction, for both rough and smooth surfaces, there are a number of secondary shocks. Comparing the two rough surfaces, the 3D lip-section appears to have a thinner downstream boundary-layer thickness than the 2D lip-section.

This thicker downstream boundary-layer, seen with the rough-surfaces in Fig. 8 and Fig. 9, reduces the "effective curvature" around the overall lip-section. This reduces the flow acceleration and results in a smaller supersonic region with a lower peak Mach number and a more, upstream, weaker, shock wave.

The difference between the downstream boundary-layer thickness can be attributed to two causes. Firstly, the growth across the SBLI and, secondly, the growth of the boundary-layer elsewhere on the surface. The similar shock location and λ-foot size for the two rough lip-sections is expected to result in a similar boundary-layer thickening across the interaction. It can be seen in the schlieren images in Fig. 8 and Fig. 9, that as the boundary-layer progresses downstream, the growth of the boundary layer is greater for the 2D roughness than the 3D roughness.

This difference in boundary-layer thickness is confirmed by the normalised boundary-layer traverses in Fig. 10, and whose extracted properties in table 3. These are taken at a location "S2", approximately at the fan-face location. When the boundary-layer profile is normalised by δ, the boundary-layer thickness, in Fig. 15, the 2D roughness and 3D roughness profiles are less full than the smooth case, and have a greater shape factor, H_i.

Comparing the two rough-surfaces with respect to the smooth surface properties, the 2D rough profile is approximately 15% thicker and slightly less full than the 3D rough profile. In the normalised plot in Fig. 11, the rough surface profiles collapse in the outer region of the boundary layer, but deviate in the region $U/U_e < 0.7$. Here, the 3D roughness boundary-layer has a slightly fuller profile. Although the momentum thickness, θ_i, within the 2D rough boundary-layer is greater than the 3D roughness, any health benefit from increased momentum is offset by the increase in boundary-layer becomes thickness. Thus there is no significant change to the health of the boundary-layer, with both rough surfaces having similar H_i values.

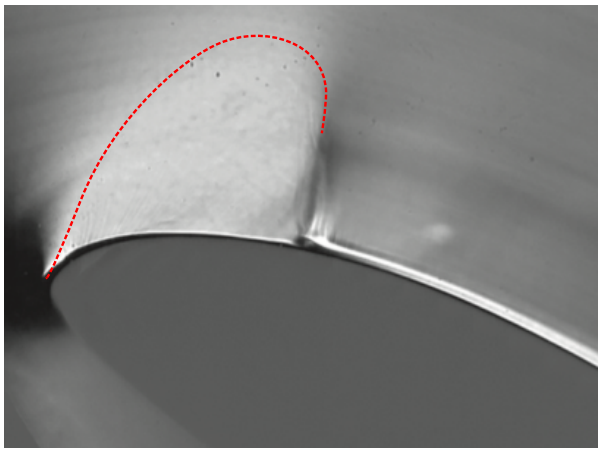

Figure 7. On-design condition, smooth lip-section. Taken from Coschignano et al.[1]

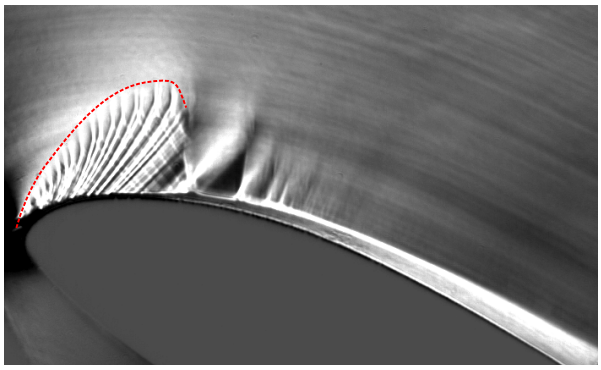

Figure 8. On-design condition, 2D roughness.

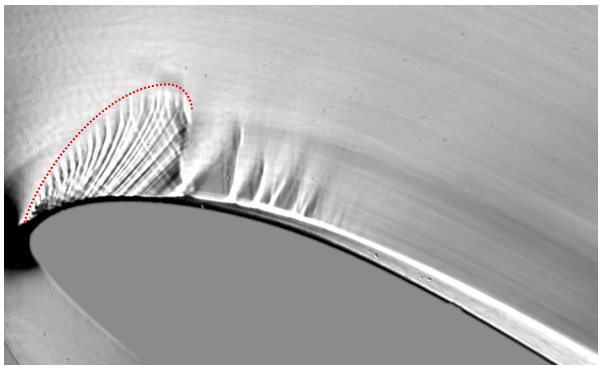

Figure 9. On-design condition, 3D roughness.

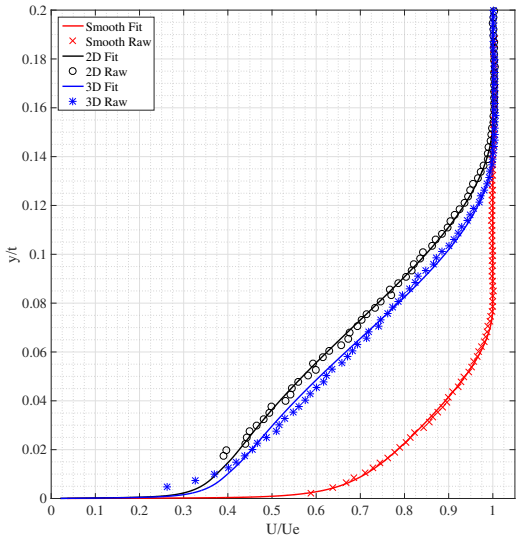

Figure 10. Boundary-layer profiles normalised by t, at location S2, on-design. Smooth results from Coschignano et al.[1]

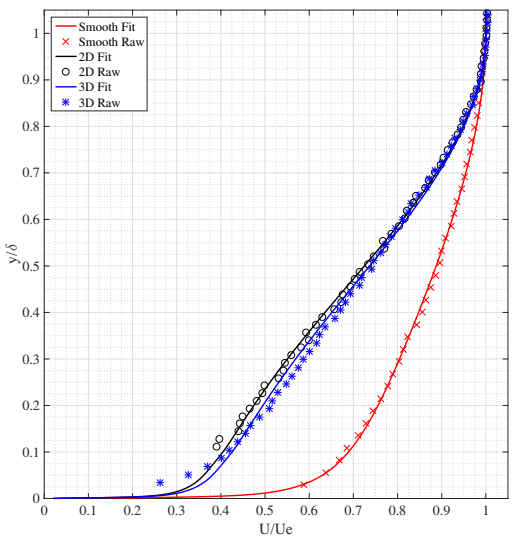

Figure 11. Boundary-layer profiles normalised by δ, at location S2, on-design. Smooth results from from Coschignano et al.[1]

Table 3. Boundary-Layer Properties at S2. Thicknesses normalised by smooth results from Coschiganano et al.[1]

Lip-section	δ/δ_s	$\delta^*/\delta^*_{i,s}$	$\theta_i/\theta_{i,s}$	H_i
Smooth	1	1	1	1.34
2D	1.99	4.14	3.01	1.84
3D	1.84	3.68	2.76	1.79

III.B. Increasing upper surface mass flow rate

Taking the lip-sections to an off-design condition, by increasing the mass flow rate over the upper surface, models an increasing mass flow demand by an engine. This changes the flow-field, seen in the schlieren images in Fig. 12.

For both the 2D and 3D rough lip-sections, increasing the mass flow rate creates a larger supersonic region, a more downstream shock location, and likely a stronger shock. The λ-foot, indicative of separation, grows in size for both rough surfaces, suggesting an increase in the extent of separation. Immediately after the interaction, the boundary-layer can be seen to be thinner with the 3D roughness compared to the 2D rough surface. Further downstream, this difference persists.

Similarly to the on-design condition, the increase in the boundary-layer thickness for both rough surfaces at a higher $\dot{m}_{upper}$ reduces the "effective curvature", which reduces the supersonic region and weakens the shock. Once again, this effect is more severe for the 2D case than the 3D case. It can be observed in the schlieren images that the 3D rough lip-section has a larger supersonic region and a shock location further downstream than the 2D roughness for each $\dot{m}_{upper}$ level. This is because the 3D rough lip-section experiences greater acceleration around the nose than the 2D lip-section roughness.

LDV traverses in Fig. 13 clearly show the movement of the shock position for an increasing $\dot{m}_{upper}$. With an increasing $\dot{m}_{upper}$, the shock is further downstream of the nose, and there is a greater drop in the Mach number, indicating an increased shock strength. With the stronger shock, there is a greater adverse pressure gradient on the boundary-layer, which creates a larger separation, and this increase in separation size is identified by the λ-foot in the schlieren images.

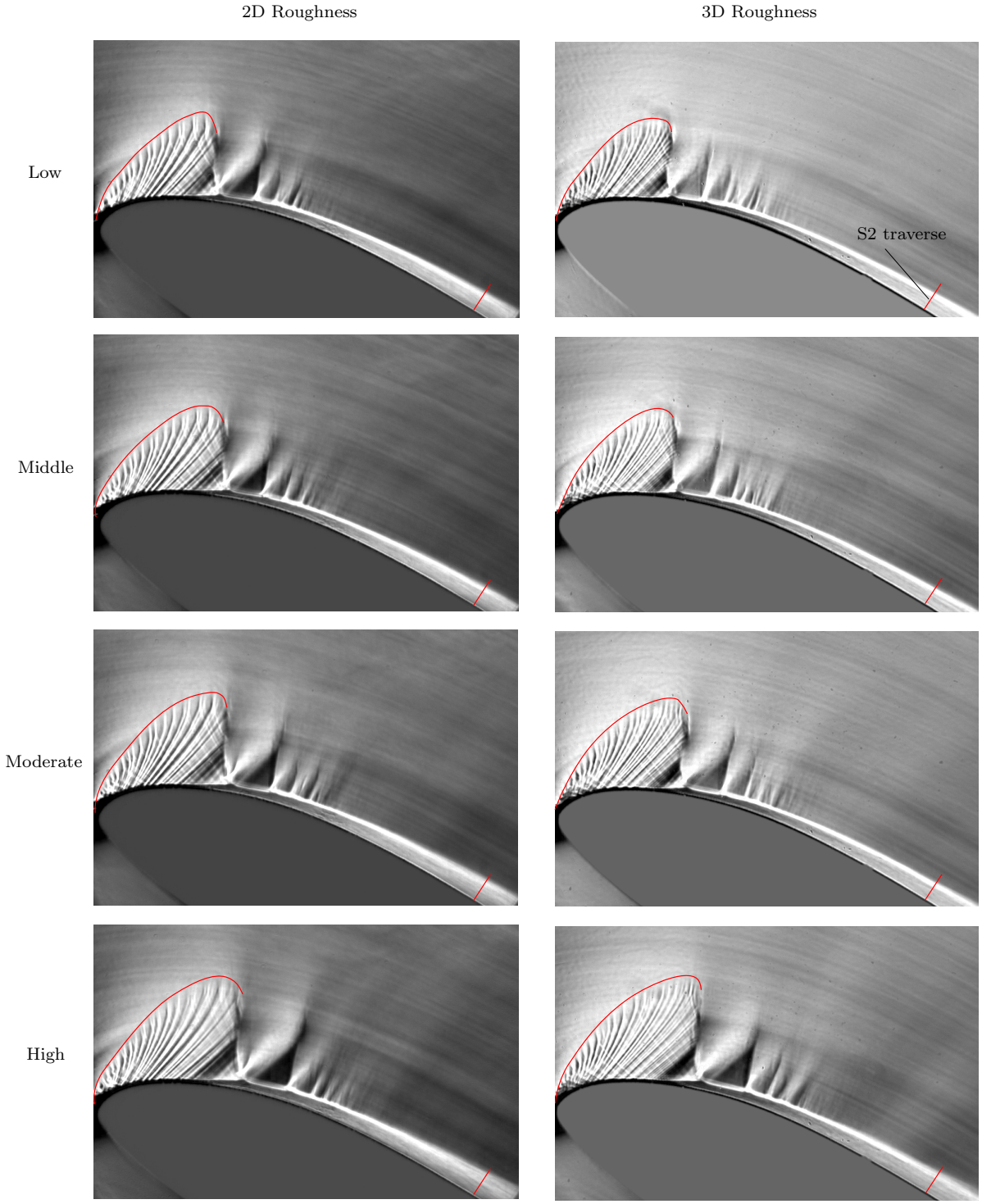

Figure 12. Comparison of Schlieren for 2D and 3D lip-sections for increasing upper surface mass flow rate

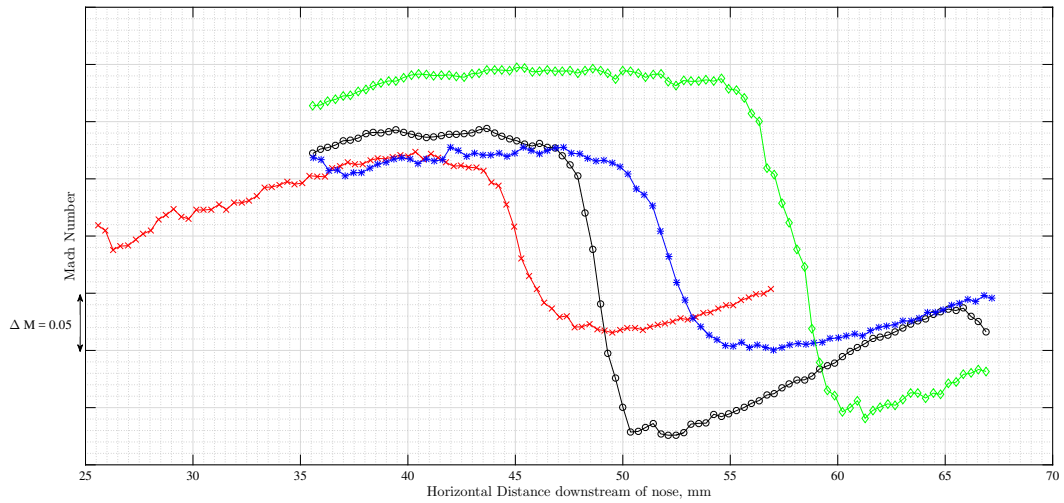

Figure 13. LDV measurements across normal shock, for 3D roughness

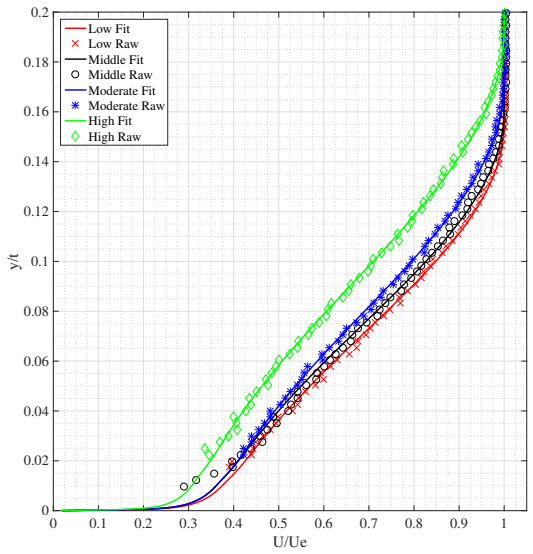

Figure 14. Boundary-layer profiles normalised by t for an increasing $\dot{m}_{upper}$, at location S2, 2D roughness.

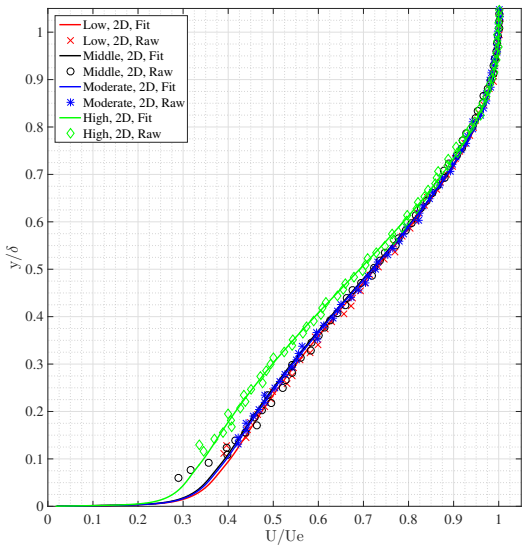

Figure 15. Boundary-layer profiles normalised by δ for an increasing $\dot{m}_{upper}$, at location S2, 2D roughness.

Table 4. Boundary-Layer properties at S2 2D roughness

$\dot{m}_{upper}$ **Level**	δ/δ_s	$\delta_i^*/\delta_{i,s}^*$	$\theta_i/\theta_{i,s}$	H_i
Low	1.99	4.14	3.01	1.84
Middle	2.06	4.38	3.14	1.88
Moderate	2.20	4.70	3.29	1.92
High	2.48	5.71	3.82	2.00

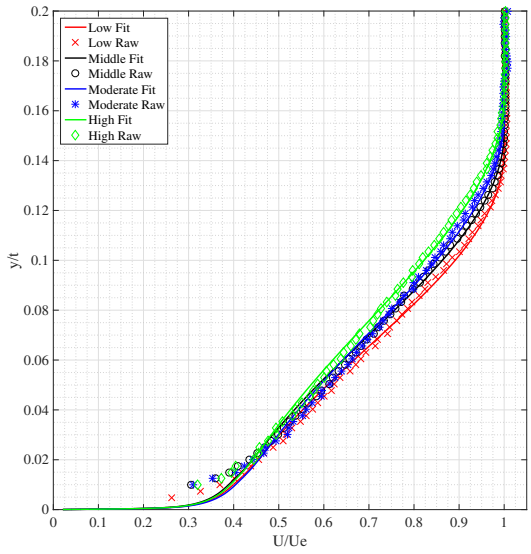

Figure 16. Boundary-layer profiles normalised by t for an increasing $\dot{m}_{upper}$, at location S2, 3D roughness.

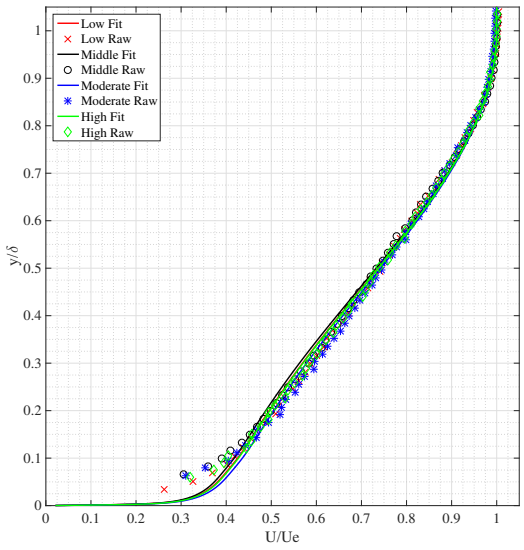

Figure 17. Boundary-layer profiles normalised by δ for an increasing $\dot{m}_{upper}$, at location S2, 3D roughness.

Table 5. Boundary-Layer properties at S2, 3D roughness

$\dot{m}_{upper}$ **Level**	δ/δ_s	$\delta_i^*/\delta_{i,s}^*$	$\theta_i/\theta_{i,s}$	H_i
Low	1.84	3.68	2.76	1.79
Middle	1.94	3.95	2.93	1.81
Moderate	2.02	3.97	3.02	1.77
High	2.13	4.26	3.20	1.79

The change in the boundary-layer thickness for each $\dot{m}_{upper}$ level is reflected in Fig. 14 and Fig. 16 for the 2D and 3D roughness respectively. The extracted boundary-layer properties in table 4 for the 2D roughness, and table 5 for the 3D roughness. These highlight that for an increasing $\dot{m}_{upper}$, there is an increase in the size of the boundary-layer thickness for both rough surfaces.

When normalised by the boundary-layer thickness, the profiles in Fig. 15 and Fig. 17 show that between the low to moderate levels of $\dot{m}_{upper}$, there is no significant change in the boundary-layer profile for both the 2D and 3D roughness.

From the moderate to the high $\dot{m}_{level}$, the two rough surface profiles are not impacted in the same manner. In Fig. 14, the 2D roughness has a much larger jump in boundary-layer thickness between the moderate to high levels, compared to the 3D roughness in Fig. 16. From the boundary-layer properties, seen in table 4 and table 5, the 2D roughness has an increase of 28% in δ/δ_s, whereas the change for the 3D roughness is 11%. This leads to a change in the profile shape when normalised.

The 2D "high" profile does not collapse onto the other three $\dot{m}_{upper}$ levels in Fig. 15 in a similar fashion to the 3D "high" profile in Fig. 17. Instead it deviates away from the collapsed curves from value of U/U_e less than 0.7. This indicates a less full, and healthy, boundary layer for the 2D roughness than the 3D roughness at this upper channel mass flow rate level.

Overall, the presence of the roughness increases the boundary-layer thickness, albeit at different rates, for an increasing upper channel mass flow rate. The two rough surfaces also have a different effect on the health of the boundary-layer. Table 4 and table 5 show the boundary-layer becoming less healthy for an increasing $\dot{m}_{upper}$ for the 2D roughness, whereas for the 3D roughness there is little change in the boundary-layer health. This difference is likely attributed to the different topologies of the roughness.

IV. Conclusions

The effect of roughness on a lip-section at incidence changes the flow-structure compared to a smooth surface lip. It promotes a smaller supersonic region and a further upstream, weaker, shock. The separation present at the base of this shock, shown by the λ-foot, is larger with roughness than with the smooth lip-section, despite the reduction in interaction strength. The boundary-layer downstream of the interaction is thicker and less healthy with the presence of roughness.

At the on-design condition, the 3D and 2D rough lip-sections have a similarly sized supersonic region and separation size. The 2D rough lip-section has greater boundary-layer growth downstream of the interaction than the 3D rough lip-section. This causes the downstream boundary-layer thickness to be thicker and less full with the 2D rough lip-section than the 3D rough lip-section at approximately the fan-face location.

The off-design operating conditions for the rough lip-sections, by increasing the $\dot{m}_{upper}$, models an increase in the demand of an engine. For both rough lip-sections, the downstream boundary-layer becomes thicker as $\dot{m}_{upper}$ increases, further reducing the "effective curvature" around the nose. The increase in the $\dot{m}_{upper}$, promotes greater acceleration around the nose, leading to a larger supersonic region and moving the shock location downstream. As the shock moves downstream it becomes stronger, increasing the size of the separation at the base of the interaction for both rough lip-sections. Compared to the smooth surface, for an increasing upper channel mass flow rate, the supersonic region is smaller for both rough surfaces.

For all $\dot{m}_{upper}$ levels, the boundary-layer is typically 10-20% thicker with the 2D roughness than the 3D roughness, at an approximate fan-face location. This boundary-layer becomes less full for the 2D rough lip-section as $\dot{m}_{upper}$ increases, but for the 3D rough lip-section, there is little change in the boundary-layer health as $\dot{m}_{upper}$ increases.

Overall, the presence of roughness promotes a thicker boundary-layer downstream of the interaction for both on-design and off-design upper channel mass flow rate conditions, leading to a smaller supersonic region and weaker shock strength, compared to a smooth surface. For these conditions, the 2D roughness has a more severe effect on the flow-field than the 3D roughness.

Acknowledgements

The authors would like to acknowledge David Martin, Sam Flint, Anthony Luckett and John Hazlewood for operating the CUED blow-down wind tunnel and Kevin Bullman for the manufacturing of the parts used in this investigation. They would also like to thank Rolls Royce Plc and the Engineering and Physical Sciences Research Council (EPSRC) for funding towards this work, and thank the National Wind Tunnel Facility.

References

[1]Coschignano, A. and Babinsky, H., "Influence of near-leading edge curvature on the performance of aero-engine intake lips at high-incidence," *34th AIAA Applied Aerodynamics Conference*, No. AIAA 2016-3559 in AIAA AVIATION Forum, American Institute of Aeronautics and Astronautics, June 2016.

[2]Coles, C., Babinsky, H., Sheaf, C., and Platt, E., "Impact of large scale roughness on aero-engines at incidence," *3AF 52nd International Conference on Applied Aerodynamics*, Lyon 2017.

[3]Herzog, J., "Rolls-Royce Trent," `http://www.wikiwand.com/en/Rolls-Royce_Trent`.

[4]Makuni, T., Babinsky, H., Slaby, M., and Sheaf, C., "Shock Wave-Boundary-Layer Interactions in Subsonic Intakes at High Incidence," No. AIAA 2015-0067, American Institute of Aeronautics and Astronautics, Jan. 2015.

[5]Kalsi, H., *Private communication*.

[6]Sun, C.-C. and Childs, M. E., "A modified wall wake velocity profile for turbulent compressible boundary layers." *Journal of Aircraft*, Vol. 10, No. 6, 1973, pp. 381–383.

[7]Musker, A. J., "Explicit expression for the smooth wall velocity distribution in a turbulent boundary layer," *AIAA Journal*, Vol. 17, June 1979, pp. 655–657.

[8]Titchener, N., Colliss, S., and Babinsky, H., "On the calculation of boundary-layer parameters from discrete data," *Exp Fluids*, Vol. 56, No. 8, Aug. 2015, pp. 159.